Webology (ISSN: 1735-188X)
Volume 19, Number 2, 2022

Synthesis Of $Ni_{1-(X)}$ $Zn_{(X)}Fe_2O_4$ Nanoparticles And Study Of Their Structure, Magnetic And Optical Properties At Different Zn^{2+}-Content

Wafa R. M. Alsuiai[1] , Bhim Sen Yadav[2] , Anchal Kishore Singh[3] , Vipul Singh[4]

[1]Department of Physics, Sam Higginbottom University of Agriculture, Technology and Sciences, Allahabad, U.P-211007, India.

[2]Department of Physics, Motilal Nehru National Institute of Technology Allahabad, Prayagraj 211004, India.

[3]Department of Physics, Motilal Nehru National Institute of Technology Allahabad, Prayagraj 211004, India.

[4]Department of Physics, Sam Higginbottom University of Agriculture, Technology and Sciences, Allahabad, U.P-211007, India.

Abstract

Composition of [$Ni_{1-(X)}Zn_{(X)}Fe_2O_4$; (X) = 0.00, 0.3, 0.5, 0.7, and 1.00] spinel nanoparticles (NPs) has been produced using sol gel auto-combustion process hardened at 800˚C for 4 hours in air. The XRD data confirm that every sample possess a spinel erection of cube phase withthe lattice constant increasing from 8.340 to 8.455 Å as Zn^{2+} ratioraises because of higher ion radii of Zn^{2+}replacing the lower ion radii of Ni^{2+}. FT-IR resul trevealed two strong absorbing bands of ferrite spinel structure and its dependence on Zn-concentration is explained and investigated. FE-SEM images revealed a nano-sized in nearly spherical-shaped element with the formation of agglomeration. The magnetic characteristics of the samples have been measured by (VSM) at R Tlater the outcomes showed that $Ni_{0.5}Zn_{0.5}Fe_2O_4$ nanoparticles present the highest M_S(saturation magnetization) of 63.3 emu/g. The direct band gap (E_g) was estimated in UV-Visible

absorption spectra and the results showed an increase in $E_g$with an increase of zinc content from 1.46 to 1.95 eV.

Keywords: Ferrite NPs, nano structured materials, reaction combustion, magnetic properties, and Optical band gap energy

1. Introduction

Mixed nickel zinc ferrite has attracted the researchers because of its categories such as high magnetic permeability, low magnetic coercivity, higher Curie temperature, high magnetization, strong resistance, lower dielectric loss, and superior mechanical strength loss, and chemical stability which makes itproper for several applications such as microwave device, magnetical storage system, magnetic fluids, telecommunication equipment's, magnetically guided drug delivery, high-frequency devices, photocatalyst, antenna rods, and gas sensor, etc. [1-6]

The mixed spinel ferrite (Ni-Zn) hasthe chemical formula $[(Zn_a^{2+}\ Fe_{1-a}^{3+})^A\ (Ni_{1-a}^{2+}Fe_{1+a}^{3+})^BO_4^{2+}\ ]$ $(0 \leq a \leq 1)$ in which the first bracket indicates (A) tetrahedral site and the second bracket indicates the (B) octahedral site. Besides that dissemination on the cations among A and B-site, the properties of such mixed ferrite are also affected by the grain size, method of preparation, chemical composition, type of substituents, holding time, and annealing temperature [7-9]

Facile combustion technique [10], co-precipitation technique [11], sol gel process [12], microwave sintering technique [13], sol gel auto-combustion technique [14], thermal deposition technique [15] and hydrothermal technique [16],are some various approaches that is used to synthesize Nickel-Zinc spinel ferrite NPs. Among all of these techniques sol gel auto-combustion, the technique has more attention due to the involvement of high purity, simple steps, homogeneous and small particle size, and low cost[17]. In this work, we have synthesized the composition of [$Ni_{1-(X)}Zn_{(X)}Fe_2O_4$: (X) = 0.00, 0.3, 0.5 0.7, and 1.00] nanoparticles and reviewed the effectivness of using Zn^{2+} ions on the structural, morphological, magnetical, as well as optical assets of nickel ferrite.

2. Experimental

2.1. Synthesis of NPssampes

The sol-gel auto-combustion approach has been utilized to make [$Ni_{1-(X)}Zn_{(X)}Fe_2$ (X) = 0.00, 0.3, 0.5, 0.7,and 1.00], Zinc ferrite spinel doped with nickel. The starting materials of nickel nitrate [$(Ni(NO_3)_2{\cdot}(6H_2O))$ - 98%],zinc nitrate [$(Zn(NO_3)_2{\cdot}(6H_2O))$ - 96%], ferric nitrate [$(Fe(NO_3)_3{\cdot}(9H_2O))$ - 98%], citric acid [$(C_6H_8O_7.\ (H_2O))$- 99%] and ammonia (NH_3)each of the analyzation grade. The metal nitrates all absorbed by distilled water in a glass beaker and agitated for 20 minutes in their stoichiometry. Then themetal nitrate (M) solution was added to (C) Citric acid (fuel) which should be stirred for 20

min. The ratio of metal nitrates (M) to total moles of citric acid (C) is adjusted at M: C = 1:1. At 70 ˚C and below constant stirring, and to maintain the (PH) value to 7 the ammonia solution is added dropped drop and then stirred continuously, inroom temperature 100°Clater, viscous gel is formed. The sol was further heated up to 200˚C. Then the auto combustion reaction occurred and loos powder was formed. Finally, the burnt powder was grounded well and toughened with in air 800˚C lasting four hours.

2.2. Characterization

The ferrite structure were studied through X-ray diffractometer (Rigaku:Smartlab 3kW) by step of 0.02°using Cu-K_α radiation (1.5406Å) in 2θ diffraction angle range from 25-70°. At room temperature, the bond structure was recorded by FTIR (Bruker: Alpha Two). Surface morphology, elemental composition characterization were investigated by FESEM (FEI: Nova Nano SEM-450) configured with EDS.At 300Kthe magnetic properties were passed out using vibrating sample magnetization (Quantum Design: Versa Lab-3Tesla). Optical absorption spectra were studied using UV-Visible (VIS) spectrometer (Shimadzu: UV_3600 Plus).

3. Result and Discussion

3.1. XRD study

The XRD pattern of all samples annealed at 800˚C indicated in Fig.1.Every peak of pure and Zn substituted Ni ferrites corresponds to JCPDS (Card-No. 44-1485 for Nickel-ferrite and Card-No. 22-1012 for Zinc-ferrite), indicating that the spinel cubic erection of ferrite has been developed. Impurity phases of Fe_2O_3 were observed for X = 0.3, 0.5, and 0.7 annealed sample (shown as ^ in Fig.1).

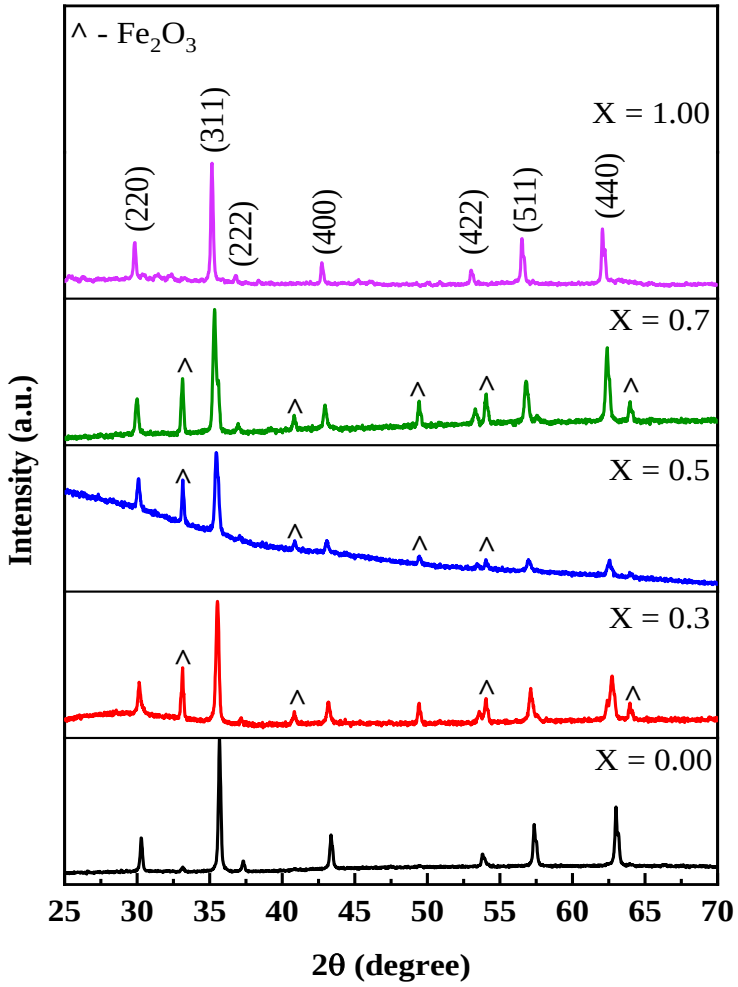

Fig. 1. XRD patterns of $Ni_{1-(X)}Zn_{(X)}Fe_2O_4$ annealed at 800˚C

The crystallite size for the highest (311) peak for all ferrite sample compositions calculated by Debye-Scherer's formula [18] is charted in table 2. Fig. 2 demonstrated the differencein crystallite size (D) as a function of Zn concentration, that lies in the range 25.61–43.95nm for different Zn content. As the concentration of the zinc rises there will be no monotonic distribution of average crystallite and this could cause a inhomogenous string and for large number of times various gel is formed and so on[19].

Zinc Content (X)	(311) peak position 2θ°	Size of Crystallite "D"(nm)	Lattice variable "a" (Å)
0	35.16	43.51	8.340
0.3	35.34	35.45	8.371
0.5	35.44	29.94	8.392
0.7	35.54	25.61	8.415
1.00	35.68	43.95	8.455

Table 1. Size of Crystallite 'D' (nm), and lattice variable'a' (Å) for Ni $_{1-(X)}Zn_{(X)}Fe_2O_4$ NPs

Using the following equation the lattice parameter 'a' is measured by miller indices (hkl) values and inter-planar spacing (d):

$$\frac{a}{d} = \sqrt{h^2 + k^2 + l^2}$$

The calculated lattice parameter 'a' for all NPs samples are listed given Table 1. The composition differentiation of lattice variable 'a' as the function of zinc content is given in Fig. 2. Fig. 2 shows a monotonic increase of lattice constant from 8.34Å to 8.455 Å by raising concentration of Zincand ascribed to the difference of ion radii of Zn^{2+} (0.83Å) which is larger than of Ni^{2+} (0.65Å)[6, 20, 21].

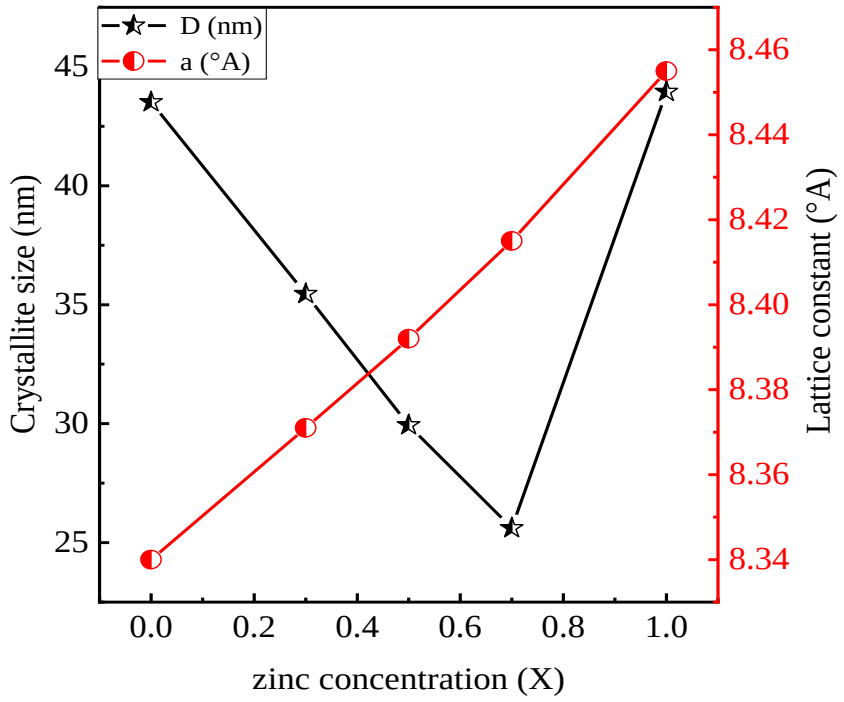

Fig. 2. Compositional variation of size of crystallite 'D' (nm) and lattice constant'a' (Å) of $Ni_{1-(X)}Zn_{(X)}Fe_2O_4$ NPs annealed at 800˚C

3.2. FT-IR measurements

Figure 3 shows FTIR measurements of all composition nanoparticles in the scale 350–4000 cm^{-1}. The weak absorption bands between 3300-3420 cm^{-1} also 1612-1629 cm^{-1} are equivalent to widening and bending vibrations of hydroxyl (O–H) group becausethe surface absorbs the water molecules [22, 23]. The bands seeming in the range (ν_1 = 560–590 cm^{-1}) and (ν_2 = 468–477 cm^{-1}) are submitted to the stretching vibrations of tetrahedral (ν_1) and octahedral (ν_2) of metal ion - oxygen (M–O) bonds [24].The frequency band at around 471 cm^{-1}isthe cause of the presence of divalent (Ni^{2+}) metal ions in octahedral (B-sites) with different forms of lattice vibration [25, 26].The FT-IR frequency bands position of increased Zn concentrationare listed in table 2. It also found that the peak position value (ν_1 and ν_2) were identified to be decreased and increased, respectively, with the increase Zn^{2+} contents except for the $ZnFe_2O_4$ sample. By addingZn^{2+} ions to tetrahedral (A- sites) that has larger radius and higher atomic mass, it causes migration inFe^{3+} to octahedral (B- sites), alsoit decreases the tetrahedral vibration frequency (ν_1). This implies increases the octahedral vibration frequency (ν_2) as a result

of the exchangein Fe^{3+} ions to the octahedral (B-site) [27,28]. The existence of these two basic bands proved the development of spinel ferrite structure of synthesized ferrites NPs [29].

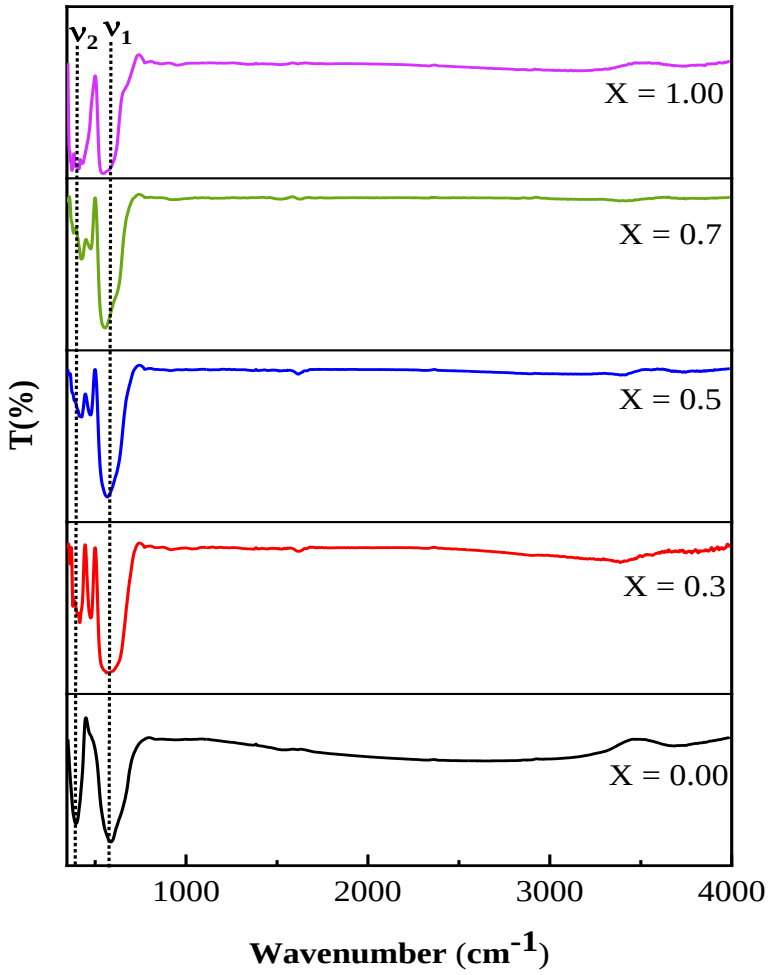

Figure 3. FT-IR spectra of $Ni_{1-(X)}\ Zn_{(X)}\ Fe_2O_4$ [X = 0.00. 0.3, 0.5, 0.7, 1.00] NPs

Zinc Content X	ν_1 [1/cm]	ν_2 [1/cm]
0.00	586	395
0.3	570	420
0.5	564	428

0.7	551	428
1.00	544	412

Table 2. FT-IR frequency bands position for tetrahedral (ν_1) and octahedral (ν_2) sites

3.3.FE-SEM with EDS

Figure 4(a-c) shows FE-SEM pictures of $Ni_{1-(X)}Zn_{(X)}Fe_2O_4$ [(X) = 0.00, 0.5, 1.00] NPs. The FESEM images of the pure nickel ferrite sample (X) = 0 show the least spherical and irregular, non-symmetrical particles andformation of agglomeration (fig4(a)). For Ni– Zn mixed ferrite sample (X) = 0.5 the agglomeration shows uniform particles with spherical shape (fig 4(b)). From fig. 4(c), the FESEM picturesindicates, that pure zinc ferrite nanoparticles (X) = 1 possess uniformity and spherical symmetry with few agglomerations. However, it is also observed that at (X) = 1 the crystallite size increase which is in decent agreement with XRD results. Figure 5 (a)-(c) shows EDS pattern of (X) = 0.00, 0.5, and 1.00 NPs. Peaks of Ni, Fe, and O were observed in pure nickel ferrite (X) = 0 sample (fig. 5(a)), and peaks corresponding to Ni, Fe, O, and Zn elements are observed in Zn-doped $NiFe_2O_4$ sample (X) = 0.5 as given in fig. 5(b). Fig. 5(c) demonstrated the peaks of Zn, O, and Fe in a pure zinc ferrite sample (X) = 1., and no other peaks were observed, which was confirmed that the annealed samples are pure and there is no other impurity.

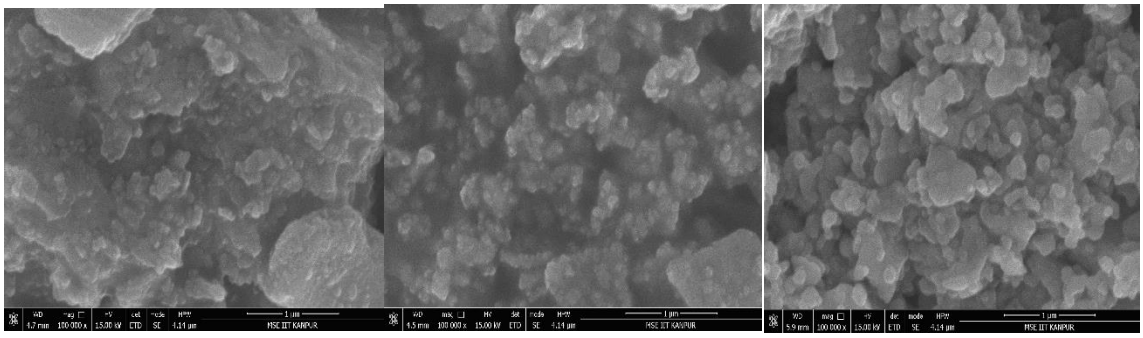

(a) (b) (c)

Figure 4. FE-SEM images for (a-c) $Ni_{1-(X)}Zn_{(X)}Fe_2O_4$ [(X)=0.00, 0.5 and 1.00] nanoparticles.

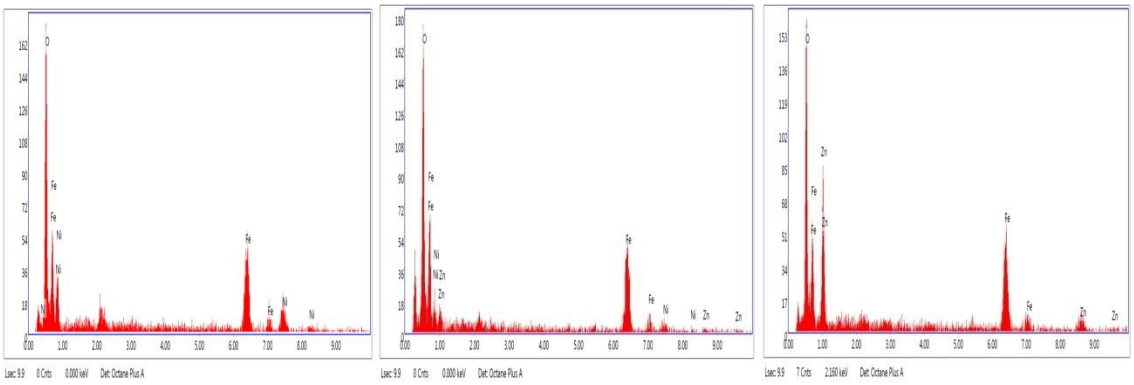

(a) (b) (c)

Figure 5. EDS spectra for (a-c) $Ni_{1-(X)}Zn_{(X)}Fe_2O_4$ [(X) = 0.00, 0.5 and 1.00] nanoparticles.

3.4. VSM (magnetic study)

Magnetic properties were performed through VSM which isan applied magnetic field of ±20kOe at 300K. Figure 6 shows (M-H) curve of synthesized all composition NPs of various Zn content. The remanent magnetization (M_R), coercive field (H_C) and saturation magnetization (M_S),values were calculated from the curves and given for different Zn concentrations in Table 3. It is noted that the M_S has no monotonic behavior as Zn content increases. It is initially increase up to (X) = 0.5 from 27 $emug^{-1}$ to 60 $emug^{-1}$later decrease to 44 $emug^{-1}$ at (X) = 0.7 and again increases to 46 $emug^{-1}$ at (X) = 1.

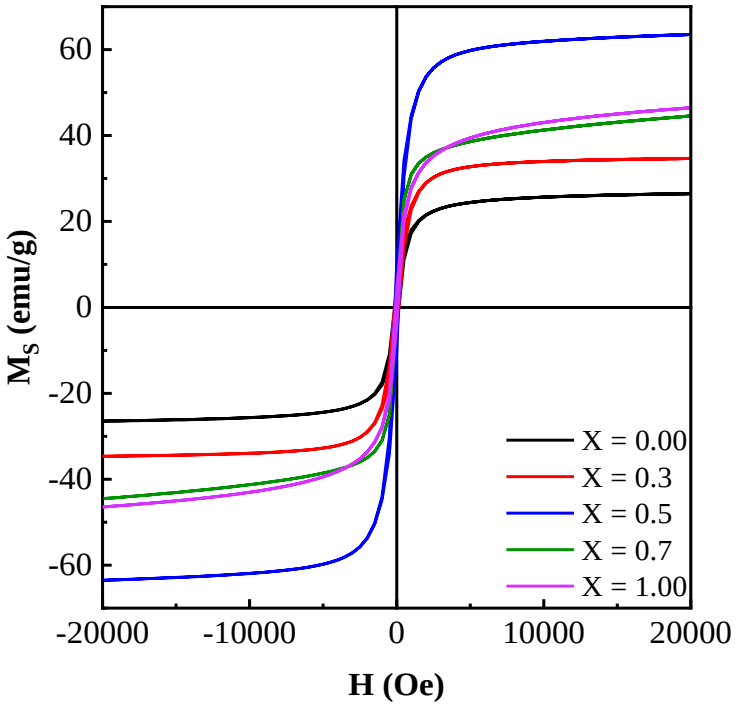

Figure 6. (M-H) loops of $Ni_{1-(X)}Zn_{(X)}Fe_2O_4$NPs sample

Zn Content (X)	M_S ($emug^{-1}$)	M_R ($emug^{-1}$)	H_C (Oe)
0.00	26.5	4.2	139
0.3	34.5	5.8	149
0.5	63.3	10.3	124
0.7	44.2	2.7	50
1.00	46.5	4.3	89

Table 3. Magnetic characteristics (M_S, M_R andH_C)of$Ni_{1-(X)}Zn_{(X)}Fe_2O_4$

The variation in saturation magnetization (M_S) wasimpacted by various factors which are crystallite size, spin canting and the exchange interaction (B-B, A-B) changes between tetrahedral(A) and octahedral (B) sub lattice [30, 31].The magnetic moment of Zn^{2+}, $Ni^{2+,}$ and Fe^{3+} are 0, 2, and 5 μ_B, y only considering spin contribution. The occupancy of non-

magnetic $Zn^{2+}(0\mu_{B)}$ substituted ions in tetrahedral (A-site) cause's transfer of $Fe^{+3}(5\mu_B)$ions from (A- site) to (B-site).This leads to the magnetic moment in tetrahedral site (A) decreasing and the increases of magnetic moment in octahedral site (B). Thus increase the net magnetization up to (X) = 0.5. This magnetic performance can be learned through Neel's model [27, 32].However the M_S decreases at (X) = 0.7. The reason forthe decrease in saturation magnetization for $Ni_{0.3}Zn_{0.7}Fe_2O_4$ NPs is that when the Zn content increase in the compound the super-exchange interaction A-B weredamaged also the octahedral spins are not held rigidly comparable to the little spins of tetrahedral sites, and thus canted spin structure occurs which causes theM_S to decrease at (X) = 0.7[33, 34]. The sample $ZnFe_2O_4$ with concentration (X) = 1 showed again an increase in.M_S.The increase in M_S at (X) = 1 was attributed as itraisesthe crystallite size of the sample.Generally,the surface to volume ratio decreasesand increases the crystallite sizewhich will lead to an increase in saturation magnetization [30, 35].Figure 7 shows the (M_S) as afunction of concentration of Zinc.Thedifference of coerivity with increased Zn^{2+} content was attributed to different factors, like domain structure, crystallite size, and magnetic crystallite anisotropy[12, 36].

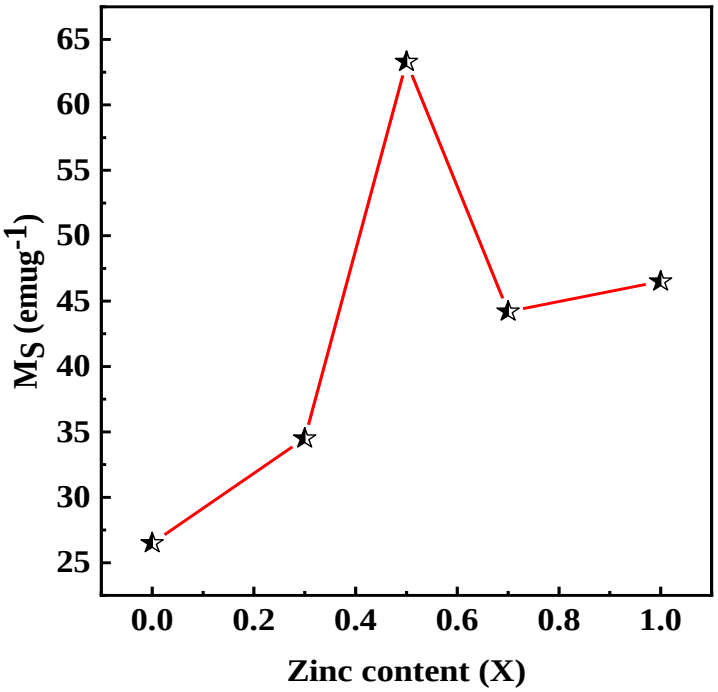

Figure 7. (M_S) as a function of zinc concentration

3.5. Optical properties

The energy band gap of all NPs weredetermined from optical absorption spectra using UV-Vis spectrometer at RT as given in figure 8.

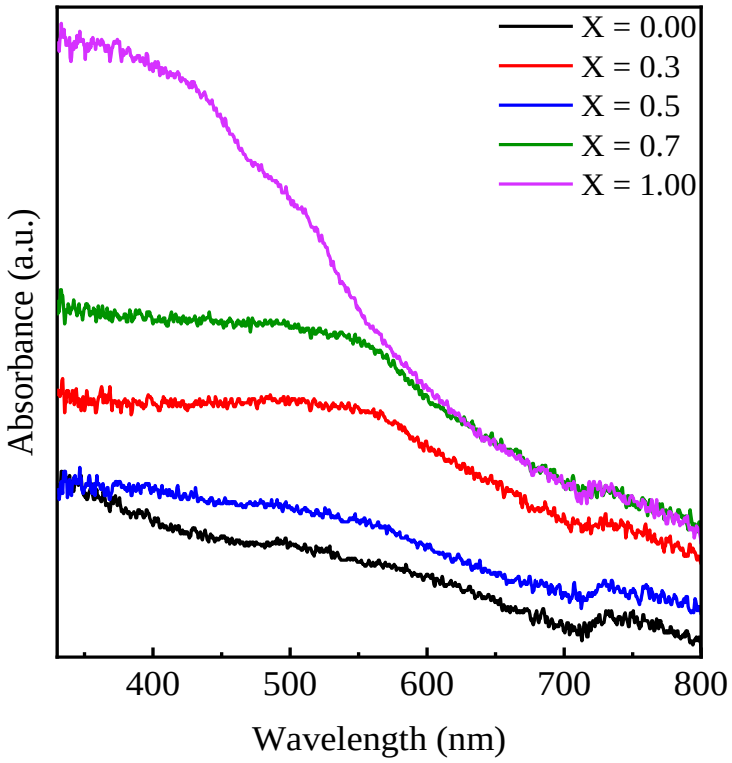

Figure 8. Absorption spectra of $Ni_{1-(X)}Zn_{(X)}Fe_2O_4$ [(X)= 0.00, 0.3, 0.5, 0.7 and 1.00] NPs

The band gap energy (Eg) values of all the samples were calculated using Taucs relation [37]:

$(\alpha h\nu) = A\,(h\nu - E_g)^n$

Where h, α, ν, A, E_g, and n are constant, light frequency, band gap energy,absorption coefficient,Planks constant, as well as exponent depend on the type of electron transition. The direct band gap (n = ½) of different Zn concentrations was estimated by linear extrapolation of plotting $(\alpha h\nu)^2$ against photon energy (hν) to the energy axis as shown in figure 9.

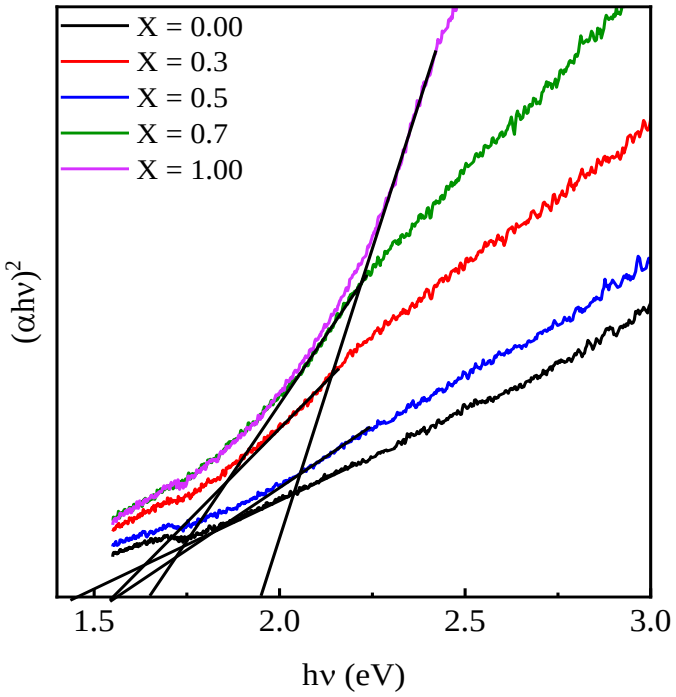

Figure 9. Tauc plot of [$Ni_{1-(X)}Zn_{(X)}Fe_2O_4$ (X) = 0.00, 0.3, 0.5, 0.7 and 1.00] NPs samples

The calculated E_g valuesof (X) = 0.00, 0.3, 0.5, 0.7 and 1.00nanoparticles are 1.46, 1.55, 1.56, 1.65, and 1.95 eV, correspondingly.The energy band gap (E_g)amountis founded to increasewith increasing Zn content that may be related toseveral factors which are crystallite size, interface effect,presence of impurity as well as structure parameter[22, 32, 38].Increasing the direct band gap for thesamples may attribute to a decrease in crystallite size (quantum size effect) [37, 39].The increase with band gap energy might be the cause of (sp-d)interchange interaction among the localized (d)electrons of (Zn^{2+})ions along with band electrons of $NiFe_2O_4$[40, 41].Note that thenarrowedbandgapvalueswith(Zn^{2+}) dopant in $NiFe_2O_4$ lattice specify the developmentin sub-bandsamongst the energy band gap and inclusion of its sub-bands along the conduction band (CB) to create a continuous band[42].

4. Conclusion

By using he sol-gel combustion approach the nano ferrites samples [$Ni_{1-(X)}Zn_{(X)}Fe_2O_4$: (X) = 0.00, 0.3, 0.5, 0.7, and 1.00]were formed. All synthesized NPs samples were annealed for 4 hours at 800˚C in the air.Thedevelopmentofcubic spinelferrite structure for allsamplesareestablished by XRD and FT-IR analyses. The lattice constant is identified to

be increased as zinc content is increasing from 8.240 Å to 8.455 Å. Magnetic properties through (VSM) indicated that $Ni_{0.5}Zn_{0.5}Fe_2O_4$ has the maximum saturation magnetization (M_S) value of 63.3 emu/g. UV-visible (Vis) spectroscopy study revealed the direct band gap of the undoped $NiFe_2O_4$ is 1.46 eV, and by increasing the Zn -content isincreasing from 1.55 to 1.95 eV.

Acknowledgment

The authors acknowledge the Centre for Interdisciplinary Research, Allahabad for providing characterizationsprovision forthe practical work and to thank Dr. Naresh Kumar, Physics Department MNNIT Allahabad, for the discussion.

References

1. Raju, P. and Murthy, S.R., 2013. Preparation and characterization of Ni–Zn ferrite+ polymer nanocomposites using mechanical milling method. Applied Nanoscience, 3(6), pp.469-475.
2. Kumar, S., Sharma, A., Singh, M. and Sharma, S.P., 2013. Simple synthesis and magnetic properties of nickel-zinc ferrites nanoparticles by using Aloe vera extract solution. Archives of Applied Science Research, 5(6), pp.145-151.
3. Sertkol, M., Köseoğlu, Y., Baykal, A., Kavas, H.Ü.S.E.Y.İ.N. and Toprak, M.S., 2010. Synthesis and magnetic characterization of $Zn_{0.7}Ni_{0.3}Fe_2O_4$ nanoparticles via microwave-assisted combustion route. Journal of Magnetism and Magnetic Materials, 322(7), pp.866-871.
4. Rashad, M.M., Elsayed, E.M., Moharam, M.M., Abou-Shahba, R.M. and Saba, A.E., 2009. Structure and magnetic properties of $Ni_xZn_{1-x}Fe_2O_4$ nanoparticles prepared through co-precipitation method. Journal of Alloys and Compounds, 486(1-2), pp.759-767.
5. Yadoji, P., Peelamedu, R., Agrawal, D. and Roy, R., 2003. Microwave sintering of Ni–Zn ferrites: comparison with conventional sintering. Materials Science and Engineering: B, 98(3), pp.269-278.
6. Yadav, A., Choudhary, P., Saxena, P., Rai, V.N. and Mishra, A., 2019. Spectroscopic analysis and temperature-dependent dielectric properties of bulk Ni–Zn ceramics. Journal of Advanced Dielectrics, 9(02), p.1950014.
7. Pratibha, G., Thirupathi, A., Krishna, V.V., Kumar, P.S., Yadav, G.S.S. and Sankara, S., 2021. Effect of Ni substitution on structural, dielectric and magnetic properties of Zn ferrite nanoparticles. Journal of Ovonic Research Vol, 17(4), pp.323-331.
8. Leng, P.L., Naseri, M.G., Saion, E., Shaari, A.H. and Kamaruddin, M.A., 2013. Synthesis and characterization of Ni-Zn ferrite nanoparticles ($Ni_{0.25}Zn_{0.75}Fe_2O_4$) by thermal treatment method. Advances in Nanoparticles, 2(4), pp.378-383.

9. Paramesh, D., Kumar, K.V. and Reddy, P.V., 2016. Influence of nickel addition on structural and magnetic properties of aluminium substituted Ni-Zn ferrite nanoparticles. Processing and Application of Ceramics, 10(3), pp.161-167.
10. Chandamma, N., Manohara, B.M., Ujjinappa, B.S., Shankarmurthy, G.J. and Kumar, M.S., 2017. Structural and electrical properties of Zinc doped Nickel ferrites nanoparticles prepared via facile combustion technique. Journal of alloys and compounds, 702, pp.479-488.
11. Kumar, A., Arora, M., Yadav, M.S. and Panta, R.P., 2010. Induced size effect on Ni doped nickel zinc ferrite nanoparticles. Physics Procedia, 9, pp.20-23.
12. Yoo, B.S., Chae, Y.G., Kwon, Y.M., Kim, D.H., Lee, B.W. and Liu, C., 2013. Effects of Solution Concentration on the Structural and Magnetic Properties of $Ni_{0.5}Zn_{0.5}Fe_2O_4$ Ferrite Nanoparticles Prepared by Sol-gel. Journal of Magnetics, 18(3), pp.230-234.
13. Sorescu, M., Diamandescu, L., Peelamedu, R., Roy, R. and Yadoji, P., 2004. Structural and magnetic properties of NiZn ferrites prepared by microwave sintering. Journal of magnetism and magnetic materials, 279(2-3), pp.195-201.
14. Kurian, M. and Nair, D.S., 2016. Effect of preparation conditions on nickel zinc ferrite nanoparticles: a comparison between sol–gel auto combustion and co-precipitation methods. Journal of Saudi Chemical Society, 20, pp.S517-S522.
15. Hwang, J., Choi, M., Shin, H.S., Ju, B.K. and Chun, M., 2020. Structural and magnetic properties of NiZn ferrite nanoparticles synthesized by a thermal decomposition method. Applied Sciences, 10(18), p.6279.
16. Majid, F., Rauf, J., Ata, S., Bibi, I., Yameen, M. and Iqbal, M., 2019. Hydrothermal synthesis of zinc doped nickel ferrites: evaluation of structural, magnetic and dielectric properties. Zeitschrift für PhysikalischeChemie, 233(10), pp.1411-1430.
17. Hedayati, K., 2015. Synthesis and characterization of nickel zinc ferrite nanoparticles. Journal of Nanostructures, 5(1), pp.13-16
18. Velmurugan, K., Venkatachalapathy, V.S.K. and Sendhilnathan, S., 2010. Synthesis of nickel zinc iron nanoparticles by coprecipitation technique. Materials Research, 13, pp.299-303.
19. Nadeem, K., Shahid, M. and Mumtaz, M., 2014. Competing crystallite size and zinc concentration in silica coated cobalt ferrite nanoparticles. Progress in Natural Science: Materials International, 24(3), pp.199-204
20. Khan, S.B., Irfan, S. and Lee, S.L., 2019. Influence of Zn^{+2} doping on Ni-based nanoferrites;(Ni1− x ZnxFe2O4). Nanomaterials, 9(7), p.1024.
21. Kumar, P., Mishra, P. and Sahu, S.K., 2011. Synthesis of Ni-Zn ferrites using low temperature sol-gel process. International Journal of Scientific & Engineering Research, 2(8).

22. Joshi, S., Kumar, M., Chhoker, S., Srivastava, G., Jewariya, M. and Singh, V.N., 2014. Structural, magnetic, dielectric and optical properties of nickel ferrite nanoparticles synthesized by co-precipitation method. Journal of Molecular structure, 1076, pp.55-62.
23. Vinosha, P.A., Mely, L.A., Jeronsia, J.E., Monica, F.H., Raja, K. and Das, S.J., 2017. Study of Structural, optical, dielectric and magnetic properties of zinc ferrite synthesized by co-precipitation. In Nano Hybrids and Composites (Vol. 17, pp. 1-9). Trans Tech Publications Ltd.
24. Chakrabarty, S., Pal, M. and Dutta, A., 2015. Structural, optical and electrical properties of chemically derived nickel substituted zinc ferrite nanocrystals. Materials Chemistry and Physics, 153, pp.221-228.
25. Shirsath, S.E., Toksha, B.G., Kadam, R.H., Patange, S.M., Mane, D.R., Jangam, G.S. and Ghasemi, A., 2010. Doping effect of Mn^{2+} on the magnetic behavior in Ni–Zn ferrite nanoparticles prepared by sol–gel auto-combustion. Journal of Physics and Chemistry of Solids, 71(12), pp.1669-1675.
26. Saafan, S.A., Meaz, T.M., El-Ghazzawy, E.H., El Nimr, M.K., Ayad, M.M. and Bakr, M., 2010. AC and DC conductivity of NiZn ferrite nanoparticles in wet and dry conditions. Journal of magnetism and Magnetic materials, 322(16), pp.2369-2374.
27. Tehrani, F.S., Daadmehr, V., Rezakhani, A.T., Akbarnejad, R.H. and Gholipour, S., 2012. Structural, magnetic, and optical properties of zinc-and copper-substituted nickel ferrite nanocrystals. Journal of superconductivity and novel magnetism, 25(7), pp.2443-2455.
28. Phor, L., Chahal, S. and Kumar, V., 2020. Zn^{2+} substituted superparamagnetic $MgFe_2O_4$ spinel-ferrites: Investigations on structural and spin-interactions. Journal of Advanced Ceramics, 9(5), pp.576-587.
29. Mohit, K., Rout, S.K., Parida, S., Singh, G.P., Sharma, S.K., Pradhan, S.K. and Kim, I.W., 2012. Structural, optical and dielectric studies of $Ni_xZn_{1-x}Fe_2O_4$ prepared by auto combustion route. Physica B: Condensed Matter, 407(6), pp.935-942.
30. Subha, A., Shalini, M.G., Rout, S. and Sahoo, S.C., 2020. Magnetic Ordering and Enhancement of Magnetization in Zinc-Substituted Copper Ferrite Nanoparticles. Journal of Superconductivity and Novel Magnetism, 33(11), pp.3577-3586.
31. Atif, M., Nadeem, M., Grössinger, R. and Turtelli, R.S., 2011. Studies on the magnetic, magnetostrictive and electrical properties of sol–gel synthesized Zn doped nickel ferrite. Journal of Alloys and Compounds, 509(18), pp.5720-5724.
32. Nawle, A.C., Humbe, A.V., Babrekar, M.K., Deshmukh, S.S. and Jadhav, K.M., 2017. Deposition, characterization, magnetic and optical properties of Zn doped $CuFe_2O_4$ thin films. Journal of Alloys and Compounds, 695, pp.1573-1582.

33. Costa, A.C.F.M., Silva, V.J., Cornejo, D.R., Morelli, M.R., Kiminami, R.H.G.A. and Gama, L., 2008. Magnetic and structural properties of $NiFe_2O_4$ ferrite nanopowder doped with Zn^{2+}. Journal of Magnetism and Magnetic Materials, 320(14), pp.e370-e372.
34. Krishna, K.R., Kumar, K.V., Ravindernathgupta, C. and Ravinder, D., 2012. Magnetic properties of Ni-Zn ferrites by citrate gel method. Advances in Materials Physics and Chemistry, 2(3), pp.149-154.
35. AnithaRani.K and Senthil Kumar.V.: Preparation and Characterization of Nickel and Copper Ferrite Nanoparticles by Sol-Gel Auto-Combustion Method. International Journa of Innovative Research in Science and engineering (2015)
36. Singhal, S., Namgyal, T., Bansal, S. and Chandra, K., 2010. Effect of Zn substitution on the magnetic properties of cobalt ferrite nano particles prepared via sol-gel route. Journal of Electromagnetic Analysis and Applications, 2010.
37. Manju, B.G. and Raji, P., 2019. Green synthesis of nickel–copper mixed ferrite nanoparticles: structural, optical, magnetic, electrochemical and antibacterial studies. Journal of Electronic Materials, 48(12), pp.7710-7720.
38. Ravindra, A.V., Chandrika, M., Rajesh, C., Kollu, P., Ju, S. and Ramarao, S.D., 2019. Simple synthesis, structural and optical properties of cobalt ferrite nanoparticles. The European Physical Journal Plus, 134(6), pp.1-10.
39. Al-Hada, N.M., Saion, E.B., Shaari, A.H., Kamarudin, M.A., Flaifel, M.H., Ahmad, S.H. and Gene, A., 2014. A facile thermal-treatment route to synthesize the semiconductor CdO nanoparticles and effect of calcination. Materials science in semiconductor processing, 26, pp.460-466.
40. Dhiwahar, A.T., Sundararajan, M., Sakthivel, P., Dash, C.S. and Yuvaraj, S., 2020. Microwave-assisted combustion synthesis of pure and zinc-doped copper ferrite nanoparticles: Structural, morphological, optical, vibrational, and magnetic behavior. Journal of Physics and Chemistry of Solids, 138, p.109257.
41. Manikandan, A., Antony, S.A., Sridhar, R., Ramakrishna, S. and Bououdina, M., 2015. A Simple Combustion Synthesis and Optical Studies of Magnetic $Zn_{1-x}Ni_xFe_2O_4$ Nanostructures for Photoelectrochemical Applications. Journal of nanoscience and nanotechnology, 15(7), pp.4948-4960.
42. Hema, E., Manikandan, A., Karthika, P., Antony, S.A. and Venkatraman, B.R., 2015. A novel synthesis of Zn^{2+}-doped $CoFe_2O_4$ spinel nanoparticles: structural, morphological, opto-magnetic and catalytic properties. Journal of Superconductivity and Novel Magnetism, 28(8), pp.2539-2552